IMPROVING PHASE-RECTIFIED SIGNAL AVERAGING FOR FETAL HEART RATE ANALYSIS

Tong Chen[⋆] *, Guanchao Feng*[⋆]*, Cassandra Heiselman*[†]*, J. Gerald Quirk*[†]*, and Petar M. Djurić*[⋆]

[⋆]Department of Electrical and Computer Engineering, Stony Brook University
[†]Department of Obstetrics/Gynecology, Renaissance School of Medicine, Stony Brook University

ABSTRACT

Low umbilical artery pH is a marker for neonatal acidosis and is associated with an increased risk for neonatal complications. Phase-rectified signal averaging (PRSA) features have demonstrated superior discriminatory or diagnostic ability and good interpretability in many biomedical applications including fetal heart rate analysis. However, the performance of PRSA-based methods is sensitive to values of the selected parameters which are usually either chosen based on a grid search or empirically in the literature. In this paper, we examine PRSA-based methods through the lens of dynamical systems theory and reveal the intrinsic connection between state space reconstruction and PRSA. From this perspective, we then introduce a new feature that can better characterize comparisons of dynamical systems with PRSA. Our experimental results on an open-access intrapartum Cardiotocography database demonstrate that the proposed feature outperforms state-of-the-art PRSA features in pH-based fetal heart rate analysis.

***Index Terms*—** phase-rectified signal averaging, fetal heart rate, dynamical system, state space reconstruction

1. INTRODUCTION

The most widely accepted approach to monitor fetal well-being during labor is by using Cardiotocography (CTG) where both fetal heart rate (FHR) and uterine activity are simultaneously recorded [1]. Although various clinical guidelines are available [2], the evaluation of FHR recordings by obstetricians suffers from high inter- and intra-variability [3]. In the computerized analysis of FHR, the gold standard for labeling FHR recordings is using the pH values of umbilical cord blood at birth, with low umbilical artery pH being a marker for neonatal acidosis and associated with an increased risk for neonatal complications [4]. A typical choice of a threshold is $\text{pH} \leqslant 7.05$. Although advanced machine learning methods, e.g., deep learning, are able to perform end-to-end learning and learn features from data automatically, such learned features and embeddings often lack interpretability. On the other hand, despite good interpretability of conventional FHR features such as features of heart rate variability, they are usually not well correlated with the pH value [5] and have limited discriminatory ability, which is often measured by the area under the receiver operating characteristic curve (AUC-ROC) of the applied method.

The phase-rectified signal averaging (PRSA) was first proposed in [6, 7] for assessing deceleration-related and acceleration-related modulations of heart rate using electrocardiogram (ECG) recordings. PRSA is robust to noise and capable of detecting quasi-periodic oscillations in non-stationary signals [8]. Therefore, it has been applied to a variety of biomedical applications including pH-based FHR analysis [9, 10], and it has been found to have superior discriminatory capability. However, the performance of PRSA is sensitive to the choice of parameters which are generally selected empirically or using a grid search. Furthermore, even for the same task, there is no consensus on appropriate values of its parameters.

Dynamical systems are often modeled using system states represented by (state) vectors that lie in their state space. Another powerful concept is the attractor of a system, which is a collection of states toward which a system tends to evolve. In reality, the attractor manifold and the mathematical description of a dynamical system are often latent, and one can only obtain some noisy, partial observations generated by the underlying system. Estimating or reconstructing an attractor manifold, i.e., state space reconstruction (SSR), is of great importance in characterizing the dynamical system and has been well studied in the literature [11]. Unlike the parameters in PRSA, well-established methods are available for selecting the parameters for SSR.

This work reveals, for the first time, the inherent connection between the PRSA and the SSR framework. To be more specific, PRSA is virtually characterizing the underlying dynamical system by averaging state vectors sampled from the reconstructed attractor manifold. This intrinsic connection is illustrated using the well-known Lorenz system. From this viewpoint, we propose a new feature, named average state distance (ASD) that is able to characterize the system in a natural manner by directly working with the reconstructed attractor manifold. In our experiments on an open access in-

This work has been supported by NIH under Award 1RO1HD097188-01.

trapartum CTG database, ASD outperformed state-of-the-art PRSA features in pH-based FHR analysis and achieved better diagnostic ability in detecting neonatal acidosis.

2. BACKGROUND

2.1. Phase-Rectified Signal Averaging

The main idea of a PRSA-based method is to quantify the average acceleration capacity (AC) and deceleration capacity (DC) of the signal. The method comprises three steps. The first step is the *anchor point selection*, where the AC anchor points (corresponding to increase events) and the DC anchor points (corresponding to decrease events) are identified. Specifically, let $x[i]$ denote the ith sample in the time series x_t, $i = 1, \ldots, N$, and $x[i]$ is an AC anchor point if

$$\frac{1}{T}\sum_{j=0}^{T-1} x[i+j] > \frac{1}{T}\sum_{j=1}^{T} x[i-j], \tag{1}$$

and it is a DC anchor point if

$$\frac{1}{T}\sum_{j=0}^{T-1} x[i+j] < \frac{1}{T}\sum_{j=1}^{T} x[i-j], \tag{2}$$

where T is a parameter for anchor point selection, and $T \ll N$. Note that, in our experiments, we adopted the definition of anchor points from [6] because, instead of converting FHR signal to RR series [10], which is the time elapsed between successive heartbeats, we directly worked with FHR signals.

In the second step, known as *phase rectifying or signal averaging step*, for each anchor point, a window of length $2L$ is constructed by taking L consecutive samples before the anchor point and $L-1$ consecutive samples after the anchor point. Then the PRSA curves for AC and DC, denoted as $\bar{\boldsymbol{x}}_{\text{AC}}$ and $\bar{\boldsymbol{x}}_{\text{DC}}$, respectively, are obtained by aligning and averaging all windows that are framed around the corresponding type of anchor points,

$$\bar{\boldsymbol{x}}[k] = \frac{1}{M}\sum_{m=1}^{M} x[i_m + k], \tag{3}$$

where M is the total number of windows associated with a specific type of anchor points, AC or DC, and $k = -L, -L+1, \ldots, 0, \ldots, L-2, L-1$ is the shift from the position of anchor point i_m in the mth window.

In the third step, named *capacity calculation step*, the AC and DC are computed by

$$\begin{aligned} \text{AC} &= \frac{1}{2s}\sum_{i=L+1}^{L+s} \bar{\boldsymbol{x}}_{\text{AC}}[i] - \frac{1}{2s}\sum_{i=L}^{L-s+1} \bar{\boldsymbol{x}}_{\text{AC}}[i], \\ \text{DC} &= \frac{1}{2s}\sum_{i=L+1}^{L+s} \bar{\boldsymbol{x}}_{\text{DC}}[i] - \frac{1}{2s}\sum_{i=L}^{L-s+1} \bar{\boldsymbol{x}}_{\text{DC}}[i], \end{aligned} \tag{4}$$

where s is a parameter for summarizing the phase-rectified curves.

2.2. The State-of-the-art of PRSA in FHR Analysis

The PRSA-based method has demonstrated superior performance and great potential for surveillance of intrauterine growth restriction and intrapartum FHR analysis [12]. In [9], the authors adopted the PRSA feature DC for pH-based FHR classification using the last 30 minutes tracings and achieved AUC-ROC of 0.665 on a large private database that contains 7568 Oxford deliveries. Recently, a new PRSA feature named deceleration reserve (DR), as a combination of DC and AC, was proposed in [10] where DR achieved AUC-ROC of 0.65 for pH-base FHR classification using the last one hour tracings on an open access intrapartum CTG database. We also adopted the same open access intrapartum CTG database in our experiments. Despite the similar performance, the parameters used in [9] and [10] are quite different. In [9], $T = 5$ and $L = 45$ (s was not reported) were selected after a grid search, whereas in [10], $T = 1$, $L = 50$, and $s = 2$ were set empirically. From a theoretical perspective, in [7], the connection between the PRSA-based method and wavelet analysis was established. In [10], the authors studied the PRSA-based method for stationary stochastic Gaussian processes and showed AC $= -$DC under such assumption.

3. MODEL DESCRIPTION

3.1. State Space Reconstruction

The Takens' theorem, proposed by Floris Takens in [13], provides theoretical guarantees that one can actually reconstruct the state space using a single observation variable of the system, when some mild conditions are satisfied. Conventionally, a reconstructed attractor manifold is called a shadow manifold.

Theorem 1 (Takens' theorem) *Let $\mathcal{M}$ be a compact manifold of (integer) dimension d. Then for generic pairs (ϕ, y), where*

- *$\phi\colon \mathcal{M} \to \mathcal{M}$ is a C^2-diffeomorphism of $\mathcal{M}$ in itself,*
- *$\mathrm{y}\colon \mathcal{M} \to \mathbb{R}$ is a C^2-differentiable function,*

the map $\boldsymbol{\Phi}_{(\phi,\mathrm{y})}\colon \mathcal{M} \to \mathbb{R}^{2d+1}$ given by

$$\boldsymbol{\Phi}_{(\phi,\mathrm{y})}(x) := \big(y(x), y(\phi(x)), y(\phi^2(x)), \ldots, y(\phi^{2d}(x))\big)$$

is an embedding of $\mathcal{M}$ in $\mathbb{R}^{2d+1}$.

In practice, a simple and popular choice of ϕ is delay-coordinate map or delay embedding. Specifically, for a time series x_t of length N, the diffeomorphic shadow manifold reconstructed from x_t with delay embedding with properly selected parameters E and τ (defined below) is denoted as $M_x := \{\mathbf{m}_x[n]\}_{n=1+\tau(E-1)}^{N}$, where

$$\boldsymbol{m}_x[n] = \big[x[n], x[n-\tau], \ldots, x[n-(E-1)\tau]\big] \tag{5}$$

is the E-dimensional (state) vector on M_x corresponding to the nth observation in x_t, i.e., $x[n]$.

It can be seen that SSR and PRSA are inherently connected. The first step in PRSA, i.e., selecting anchor points, in a time series x_t can be seen as irregularly sampling the shadow manifold M_x reconstructed with $E = 2L$ and $\tau = 1$. The second step in PRSA, i.e., the phase rectifying or signal averaging step, can be seen as calculating the averaged AC and DC system state vectors denoted as $\boldsymbol{m}_x^{\text{AC}} \in \mathbb{R}^{2L}$ and $\boldsymbol{m}_x^{\text{DC}} \in \mathbb{R}^{2L}$, respectively. Finally, the capacity calculation step of PRSA is essentially characterizing shadow manifold by summarizing the system state vectors $\boldsymbol{m}_x^{\text{AC}}$ and $\boldsymbol{m}_x^{\text{DC}}$.

The delay embedding dimension E is usually determined with false-nearest-neighbors (FNN) algorithm by examining how the number of neighbors (of a point along a signal trajectory) changes as a function of embedding dimension [14]. FNN selects E as the smallest embedding dimension that minimizes the number of false neighbors. The delay τ is a free parameter, and in theory, its value can be arbitrarily selected. However, in reality, since time series are of finite length, the choice of τ also affects the SSR quality. If τ is small, the dimensions in the shadow manifold will be highly correlated, whereas if τ is too large, dynamical information may be missed. In practice, τ is often selected to be the delay that achieves the first local minimum of the average mutual information (AMI) [15] or cross correlation between the original time series and its delayed version. In this work, we utilized delay embedding for SSR, where E and τ were selected using FNN [14] and the AMI-based method [15], respectively.

3.2. State Vector Clustering

In PRSA, the anchor points are selected with criteria (specified by the value of T) on a given time series x_t. In the literature, T is often selected to be relatively small, e.g., $T = 1$, for capturing oscillations. As a result, the majority of observations in x_t are either AC or DC anchor points. Since there is an one-to-one mapping from $x[n]$ to $\boldsymbol{m}_x[n]$, PRSA essentially assigns majority of system states to have either AC or DC status. Despite efforts for theoretical analysis of PRSA, selecting an appropriate T (especially jointly with L and s) for a specific task and dataset remains challenging. Besides, anchor points that are of the same type are not necessarily having similar system states. Therefore, instead of designing and optimizing the AC or DC anchor point selection criteria for different tasks and datasets, we directly work with state space using shadow manifold M_x and cluster the state vectors in M_x (i.e., rows of M_x) into two classes so that the similarity in state space is properly preserved. Essentially, M_x is partitioned into $M_x^{\text{cluster 1}} \in \mathbb{R}^{N_1 \times E}$ (denotes the collection of state vectors in cluster 1) and $M_x^{\text{cluster 2}} \in \mathbb{R}^{N_2 \times E}$ (denotes the collection of state vectors in cluster 2). In this work, we adopted K-means clustering [16] with the Euclidean distance as a distance measure for its simplicity, although more sophisticated clustering methods can readily be applied.

3.3. Average State Distance

The average state vector of cluster 1 denoted as $\mathbf{m}_x^{\text{cluster 1}} \in \mathbb{R}^E$, can be constructed by the mean value of each column in $M_x^{\text{cluster 1}}$. Similarly, $\mathbf{m}_x^{\text{cluster 2}} \in \mathbb{R}^E$ is calculated by averaging each column of $M_x^{\text{cluster 2}}$. Finally, we define the average state distance (ASD) of x_t as in (6) to characterize M_x, which is the Euclidean distance between $\mathbf{m}_x^{\text{cluster 1}}$ and $\mathbf{m}_x^{\text{cluster 2}}$,

$$\text{ASD}(x_t) = \left\| \mathbf{m}_x^{\text{cluster 1}} - \mathbf{m}_x^{\text{cluster 2}} \right\|. \tag{6}$$

4. EXPERIMENTS AND RESULTS

4.1. Simulated Data: Lorenz System

To demonstrate the intrinsic connection between the PRSA-based method and SSR, we adopted the well-studied Lorenz system [17], described by

$$\begin{aligned} dx/dt &= \sigma(y - x), \\ dy/dt &= x(\rho - z) - y, \\ dz/dt &= xy - \beta z. \end{aligned} \tag{7}$$

A Lorenz attractor $\mathcal{M}$ of length $N = 921$ was simulated with (7) using a classic set of parameter values $\sigma = 10$, $\rho = \frac{8}{3}$, and $\beta = 28$. We assumed only x_t was observed.

We implemented the anchor point selection of PRSA-based method on x_t (with $T = 5$ and $L = 20$) and K-means clustering on the shadow manifold M_x (reconstructed with $\tau = 1$ and $E = 40$), respectively. We set $E = 40$ and $L = 20$ so that the window length in PRSA and SSR are the same. Since the observations x_t are tested one by one in the anchor point selection, $\tau = 1$ was used to match with this behavior of PRSA. The shadow manifold $M_x \in \mathbb{R}^{882 \times 40}$ was high dimensional and thus could not be plotted directly. Instead, it was visualized with a Gaussian process latent variable model (GPLVM), which can be used for visualizing high dimensional data using nonlinear dimensionality reduction [18]. Specifically, M_x was compressed or reduced to $M_x^{\text{GP}} \in \mathbb{R}^{882 \times 3}$ and the nonlinear mapping between M_x and M_x^{GP} was governed by a Gaussian process (GP). More details for GPLVM can be found in [18].

The connection between PRSA and SSR is illustrated in Fig. 1. For the PRSA-based method (Fig. 1a), anchor points in x_t were selected first, and then for each anchor point, we colored the corresponding state vector in shadow manifold based on its type (AC or DC). In contrast, for our method (Fig. 1b), we directly clustered the state vectors in the shadow manifold, and then colored the observations in x_t based on the clustering results of their corresponding state vectors. It can be seen that selecting the anchor points in x_t is essentially (irregularly) sampling and clustering the state vectors in M_x. By directly working with state vectors in the shadow manifold, the similarity of states can be better preserved, which is often of better interpretability. For example, in Fig. 1b, the state vectors on the left lobe were assigned to one class and the ones on the right lobe were assigned to the other class.

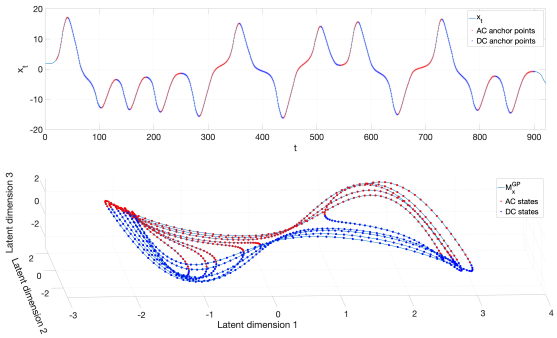

(a) DC and AC anchor points selected in x_t with $T = 5$ and $L = 20$ (top) and their corresponding states vectors in shadow manifold (bottom) where the state vectors were colored based on the type of their corresponding anchor points selected using PRSA.

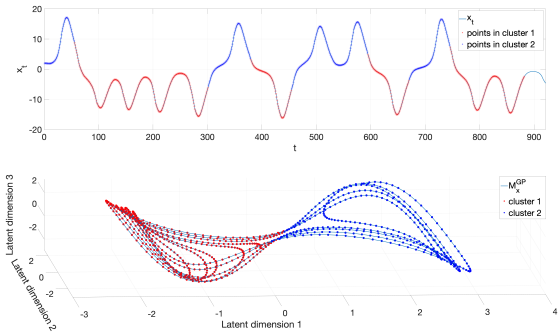

(b) Different from PRSA, in our method, we first applied K-means clustering of state vectors in the shadow manifold and colored them based on the cluster they belong to (bottom). Then the observations in x_t were colored based on the clustering results (top).

Fig. 1: Comparison between PRSA and the proposed approach using simulated data.

Table 1: Summary of performance of PRSA features

		AUC-ROC			
		FHR		RR series (in ms)	
$T = 5, L = 45$ [9]	AC	$s = 45$	0.5963	$s = 2$	0.4872
	DC	$s = 2$	0.4732	$s = 45$	**0.6066**
	DR	$s = 2$	0.4827	$s = 40$	0.5661
$T = 1, L = 50$, $s = 2$ [10]	AC	**0.5325**		0.4901	
	DC	0.4787		0.5054	
	DR	0.5069		0.4932	

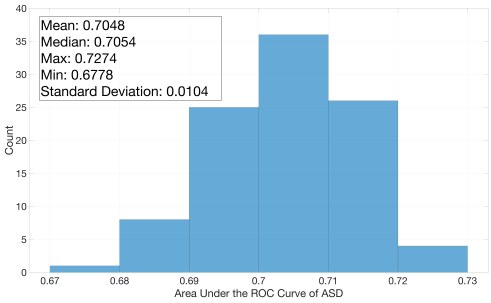

Fig. 2: Histogram of AUC-ROC of ASD over 100 runs on the open access intrapartum CTG database.

4.2. Real Data: Open Access Intrapartum CTG Database

In this section, we adopted the same open access intrapartum CTG database [19] that was used in [10], and compared the performance of ASD and state-of-the-art PRSA features in [9] and [10]. This database contains 552 recordings as well as the corresponding pH values of umbilical cord blood at birth. Both FHR and UA signals were sampled at 4Hz. We used the same labeling approach as in [9] and [10], where the positive cases are the FHR recordings associated with pH $\leqslant 7.05$.

In our experiments, similar to [9], the last 30 minutes of FHR recordings were used. Since RR series were employed in [10], we computed the PRSA features on both FHR recordings and RR series (in milliseconds). For benchmarking purposes, we extracted AC and DC using the parameters reported in [9, 10], and additionally computed DR proposed in [10]. Similar to [9,10], AUC-ROC was used as a performance metric. The performance of the PRSA features is summarized in Table 1. Note that, the parameter s was not specified in [9], so a grid search was performed for s and the highest AUC-ROC score and the corresponding s are reported.

To properly account for the randomness introduced by K-means clustering (as it initializes centroids randomly), we repeated the experiment of ASD on the open access intrapartum CTG database 100 times. The histogram of AUC-ROC of ASD over 100 runs and some statistics are shown in Fig. 2. The result clearly shows that the ASD outperformed the state-of-the-art PRSA features summarized in Table 1 and demonstrated better diagnostic ability for neonatal acidosis; the mean and median of AUC-ROC of ASD are both around 0.705, and the standard deviation is only around 0.01.

5. CONCLUSIONS

In this work, we generalize PRSA-based method by casting it in the SSR framework and show that it is essentially sampling shadow manifold and summarizing certain state vectors. Then we propose a new feature, named ASD, that is able to summarize the shadow manifold more naturally. Our results show that ASD is of superior diagnostic ability for neonatal acidosis compared to state-of-the-art PRSA features. Further, the proposed approach can be readily applied for signal analysis in other fields. Natural signals are generated by low dimensional systems [20], and the proposed method can be combined with a dimensionality reduction method when high dimensional shadow manifolds are encountered.

6. REFERENCES

[1] Antoniya Georgieva, Patrice Abry, Václav Chudáček, Petar M Djurić, Martin G Frasch, René Kok, Christopher A Lear, Sebastiaan N Lemmens, Inês Nunes, Aris T Papageorghiou, et al., "Computer-based intrapartum fetal monitoring and beyond: A review of the 2nd workshop on signal processing and monitoring in labor (October 2017, Oxford, UK)," *Acta Obstetricia et Gynecologica Scandinavica*, vol. 98, no. 9, pp. 1207–1217, 2019.

[2] Diogo Ayres-de Campos, Catherine Y Spong, Edwin Chandraharan, and FIGO Intrapartum Fetal Monitoring Expert Consensus Panel, "FIGO consensus guidelines on intrapartum fetal monitoring: Cardiotocography," *International Journal of Gynecology & Obstetrics*, vol. 131, no. 1, pp. 13–24, 2015.

[3] Lukáš Hruban, Jiří Spilka, Václav Chudáček, Petr Janků, Michal Huptych, Miroslav Burša, Adam Hudec, Marian Kacerovskỳ, Michal Kouckỳ, Martin Procházka, et al., "Agreement on intrapartum cardiotocogram recordings between expert obstetricians," *Journal of Evaluation in Clinical Practice*, vol. 21, no. 4, pp. 694–702, 2015.

[4] A Bonnaerens, A Thaens, T Mesens, C Van Holsbeke, ETM De Jonge, and W Gyselaers, "Identification of neonatal near miss by systematic screening for metabolic acidosis at birth," *Facts, Views & Vision in ObGyn*, vol. 3, no. 4, pp. 281, 2011.

[5] Guanchao Feng, J Gerald Quirk, and Petar M Djurić, "Extracting interpretable features for fetal heart rate recordings with Gaussian processes," in *2019 IEEE 8th International Workshop on Computational Advances in Multi-Sensor Adaptive Processing (CAMSAP)*. IEEE, 2019, pp. 381–385.

[6] Jan W Kantelhardt, Axel Bauer, Aicko Y Schumann, Petra Barthel, Raphael Schneider, Marek Malik, and Georg Schmidt, "Phase-rectified signal averaging for the detection of quasi-periodicities and the prediction of cardiovascular risk," *Chaos: An Interdisciplinary Journal of Nonlinear Science*, vol. 17, no. 1, pp. 015112, 2007.

[7] Axel Bauer, Jan W Kantelhardt, Armin Bunde, Petra Barthel, Raphael Schneider, Marek Malik, and Georg Schmidt, "Phase-rectified signal averaging detects quasi-periodicities in non-stationary data," *Physica A: Statistical Mechanics and its Applications*, vol. 364, pp. 423–434, 2006.

[8] Quan Liu, Yi-Feng Chen, Shou-Zen Fan, Maysam F. Abbod, and Jiann-Shing Shieh, "Quasi-periodicities detection using phase-rectified signal averaging in EEG signals as a depth of anesthesia monitor," *IEEE Transactions on Neural Systems and Rehabilitation Engineering*, vol. 25, no. 10, pp. 1773–1784, 2017.

[9] Antoniya Georgieva, A.T. Papageorghiou, S. Payne, M Moulden, and CWG Redman, "Phase-rectified signal averaging for intrapartum electronic fetal heart rate monitoring is related to acidaemia at birth," *BJOG: An International Journal of Obstetrics & Gynaecology*, vol. 121, 02 2014.

[10] Massimo Walter Rivolta, Tamara Stampalija, Martin G Frasch, and Roberto Sassi, "Theoretical value of deceleration capacity points to deceleration reserve of fetal heart rate," *IEEE Transactions on Biomedical Engineering*, vol. 67, no. 4, pp. 1176–1185, 2019.

[11] James C Robinson, "A topological delay embedding theorem for infinite-dimensional dynamical systems," *Nonlinearity*, vol. 18, no. 5, pp. 2135, 2005.

[12] Evelyn Huhn, Silvia Lobmaier, Thorsten Fischer, Raphael Schneider, Axel Bauer, Karl Schneider, and Georg Schmidt, "New computerized fetal heart rate analysis for surveillance of intrauterine growth restriction," *Prenatal Diagnosis*, vol. 31, pp. 509–14, 05 2011.

[13] Floris Takens, "Detecting strange attractors in turbulence," in *Dynamical Systems and Turbulence, Warwick 1980*, pp. 366–381. Springer, 1981.

[14] Carl Rhodes and Manfred Morari, "False-nearest-neighbors algorithm and noise-corrupted time series," *Physical Review E*, vol. 55, no. 5, pp. 6162, 1997.

[15] Holger Kantz and Thomas Schreiber, *Nonlinear time series analysis*, vol. 7, Cambridge University Press, 2004.

[16] Christopher M Bishop, "Pattern recognition," *Machine Learning*, vol. 128, no. 9, 2006.

[17] Edward N Lorenz, "Deterministic nonperiodic flow," *Journal of Atmospheric Sciences*, vol. 20, no. 2, pp. 130–141, 1963.

[18] Neil D Lawrence, "Gaussian process latent variable models for visualisation of high dimensional data.," in *Nips*. Citeseer, 2003, vol. 2, p. 5.

[19] Václav Chudáček, Jiří Spilka, Miroslav Burša, Petr Janků, Lukáš Hruban, Michal Huptych, and Lenka Lhotská, "Open access intrapartum CTG database," *BMC Pregnancy and Childbirth*, vol. 14, no. 1, pp. 1–12, 2014.

[20] Graham Heimberg, Rajat Bhatnagar, Hana El-Samad, and Matt Thomson, "Low dimensionality in gene expression data enables the accurate extraction of transcriptional programs from shallow sequencing," *Cell Systems*, vol. 2, no. 4, pp. 239–250, 2016.